



Mesoporous silica-coated gold nanorods with a thermally responsive polymeric cap for near-infrared-activated drug delivery

Zhixuan Song¹ , Jun Shi^{1,*} , Zheng Zhang¹ , Zeer Qi¹ , Shangru Han¹ , and Shaokui Cao^{1,*} 

¹ School of Materials Science and Engineering, Zhengzhou University, Zhengzhou 450001, People's Republic of China

Received: 14 November 2017

Accepted: 5 February 2018

Published online:
13 February 2018

© Springer Science+Business Media, LLC, part of Springer Nature 2018

ABSTRACT

In this work, gold nanorods (AuNRs)/mesoporous silica (SiO₂) nanoparticles capped with thermal-responsive polymer were fabricated to couple the photothermal property of AuNRs and the thermal-/pH-responsive properties of polymer in a single nanovehicle. Aliphatic poly(urethane-amine) (PUA) was employed as the smart polymer to cap the mesopores of AuNRs/SiO₂ nanoparticles via in situ polymerization in supercritical CO₂. Thermal-/pH-responsive PUA acted as the on-off switch to control the DOX release due to the stretch and shrinkage of the PUA polymer chains at different temperatures, whereas a remote near-infrared (NIR) light was used to activate the phase change and subsequent drug release. The in vitro drug release studies indicated that Au/SiO₂/PUA nanoparticles exhibited distinguished pH-, thermal-, and NIR-dependent release properties. A short time exposure to NIR irradiation could distinctly increase the local temperature of nanoparticles, and the thermal-responsive polymeric cap enabled the DOX release in a significant reversible way by simply adjusting the NIR laser intensity. The present paper provides an ideal way to fabricate NIR-responsive drug carriers by combining stimuli-responsive polymer with inorganic matrix, which is highly attractive for remote controllable drug delivery.

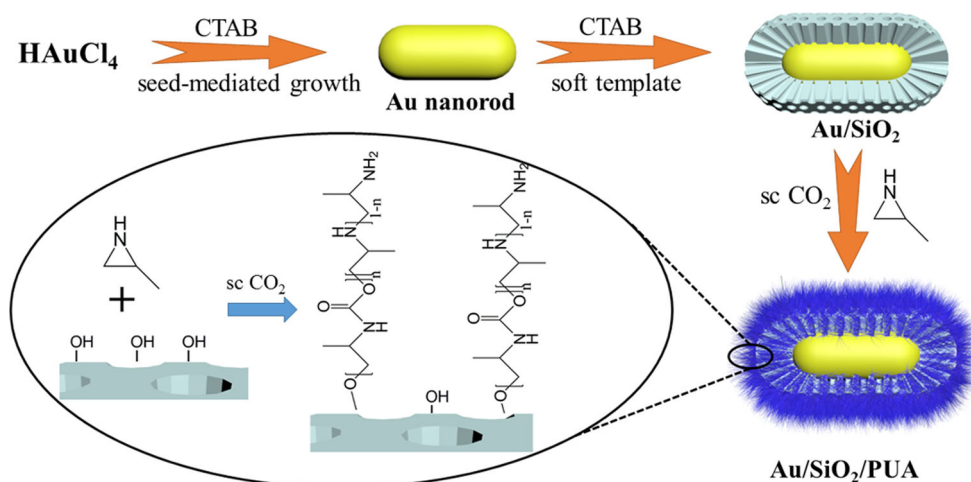
Introduction

During the past decades, smart drug delivery system (DDS) has attracted increasing attention because it can deliver drug more precisely and intelligently, which is one of the most hopeful approaches to improve the cancer therapy [1, 2]. Anchoring

functional polymers on certain inorganic nanomaterials has resulted in the design of “smarter” DDS including nano-sized vectors [3] and synthetic macromolecule [4, 5]. More importantly, polymers show outstanding advantages in attaching other ligands and increasing biocompatibility of drug delivery matrix. One such particular example of DDS was the development of so-called phototriggered

Address correspondence to E-mail: shijun@zzu.edu.cn; caoshaokui@zzu.edu.cn

Scheme 1 Preparation of Au/SiO₂/PUA nanoparticles.



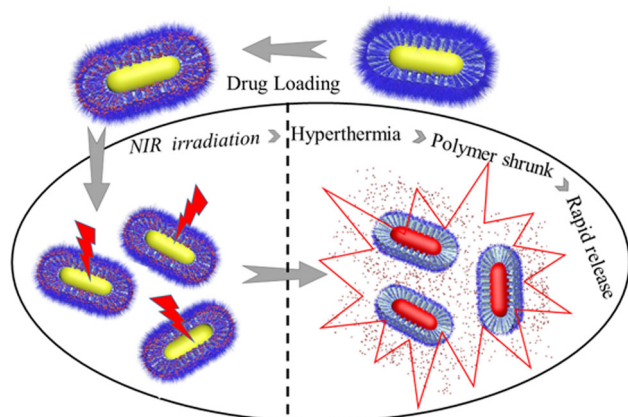
theranostic nano-platforms [6], which could realize detection, therapy, and even monitor simultaneously by assembling polymer with instinct function into one single nanovehicle [7].

Among all those nano-platforms, various mesoporous silica-coated gold nanorods (Au/SiO₂) [8] have been an excellent candidate in smart DDS [9, 10]. The surface modification of Au/SiO₂ [11, 12] is an efficient way to obtain specific properties and improve the surface activities of Au/SiO₂ [13, 14]. In recent years, many efforts have been devoted to introducing gating moieties [15, 16] in order to regulate the release behaviors of SiO₂-based DDS [17], such as the use of small organic molecules [18, 19], supramolecular assemblies [20], and liposomes [21]. Zhang et al. synthesized the hybrid Au/SiO₂ core-shell structure capped with pure poly(N-isopropylacrylamide) (PNIPAAm), and the hybrid materials could be used in thermo-chemotherapy. PNIPAAm, as a most widely studied thermal-responsive polymer [22, 23], has been extensively employed in smart biomedical area [24]. However, the poor degradability and potential cytotoxicity of PNIPAAm would bring side effects on the bioactive substance. Aliphatic poly(urethane-amine) (PUA), consisting of hydrophobic urethane and hydrophilic amine unites, shows a thermally induced reversible transition and excellent pH-responsive property as illustrated in Figure S1† of the Supporting Information.† Compared with PNIPAAm, aliphatic PUA can adjust its lower critical solution temperature (LCST) by shifting the proportion of the hydrophobic urethane and hydrophilic amine unites, which has a great potential in drug delivery area for its thermal-/pH-

responsiveness, flexibility, biodegradability, biocompatibility, and non-cytotoxicity [25, 26].

Herein, we design a novel approach to prepare smart Au/SiO₂/PUA nanoparticles via in situ functionalization of Au/SiO₂ with thermal-responsive aliphatic PUA in supercritical CO₂, as shown in Scheme 1. Basically, gold nanorods (AuNRs) [27, 28] could absorb near-infrared (NIR) light and convert it into heat efficiently to induce local hyperthermia [29]. The introduction of mesoporous silica [20, 30, 31] shell brought high specific surface area, well-defined ordered mesostructure, and good biocompatibility. Compared to conventional polymerization, the present paper avoided the application of organic solvents, and eco-friendly CO₂ was used as solvent and reactant in the polymerization reaction. In addition, PUA could be grafted successfully onto the mesopores of silica shells due to the strong diffusibility of scCO₂. More importantly, covalent bonds between aliphatic PUA and SiO₂ matrix formed by the amino groups and the hydroxyl groups increased the overall stability of nanoparticles effectively. Therefore, there were enough reasons to deduce that aliphatic PUA as a substitution could bring more potential advantages for the application in biomedicine field.

In the present design, aliphatic PUA was employed as a reversible thermal-responsive cap due to the shrinkage and stretch of PUA polymeric chains at different temperatures, whereas a remote NIR light was used to activate the phase change and subsequent drug release, as shown in Scheme 2. Specifically, when the temperature was below the LCST, the swelled PUA chains sealed the release channels and the gate was in off position, which resulted in the



Scheme 2 Thermal-/NIR-responsive drug release properties of Au/SiO₂/PUA.

slow release of doxorubicin hydrochloride (DOX). When the temperature was over the LCST, the PUA chains shrunk and the mesopores of SiO₂ were open, which resulted in the rapid release of DOX. More interestingly, it was deserved to emphasize that the reversible phase change of PUA not only introduced the thermal-responsive drug release behavior to Au/SiO₂ nanoparticles, but also endowed the nanoparticles with distinguished reversible on–off release properties when exposing the nanoparticles to NIR irradiation, as illustrated in Scheme 2. The present paper provides a green and facile route to fabricate a smart core–shell nanovehicle by integrating thermal-responsive PUA with Au/SiO₂ matrix, which is highly attractive for remote controllable drug delivery.

Experimental

Materials

Doxorubicin hydrochloride (DOX, Beijing Hua-fenglianbo Chemical, China), DL-1-amine-2-propanol (Aladdin Reagent Co. Ltd, China), chloroauric acid tetrahydrate (HAuCl₄·4H₂O, Sinopharm Chemical Reagent Co., China), tetra-ethylorthosilicate (TEOS, Tianjin Kermel Chemical, China), cetyltrimethylammonium bromide (CTAB, Tianjin Kermel Chemical, China), silver nitrate (AgNO₃, Aladdin Reagent Co. Ltd, China), sodium borohydride (NaBH₄, Tianjin Kermel Chemical, China), and ascorbic acid (AA, Tianjin Kermel Chemical, China) were analytical

reagents and used as received. Commercial CO₂ (99.999% pure) was used without further purification.

Preparation of Au/SiO₂

AuNRs were fabricated by the classical El-Sayed method [32] with some minor modifications. A CTAB solution (9.9 mL, 200 mM) was mixed with a HAuCl₄ solution (0.1 mL, 25 mM). An ice-cold NaBH₄ solution (0.6 mL, 10 mM) was injected into the mixed solution rapidly to form seed solution. The growth solution was prepared by mixing CTAB (98 mL, 200 mM), HAuCl₄ (2 mL, 25 mM), and AgNO₃ (2.5 mL, 4 mM). Once the solution became colorless after the addition of ascorbic acid (0.7 mL, 78.8 mM), the seed solution (1 mL) was added immediately. Finally, AuNRs solution was obtained after standing the growth solution for 6 h.

Au/SiO₂ nanoparticles were prepared via Matsuura protocol with some modifications [33]. After turning the pH of AuNRs dispersion in deionized water to around 10 by adding NaOH, 200 μL of 25% TEOS in methanol was added slowly under gentle stirring. The reaction was kept at 30 °C for 2 days. The product was washed by water centrifugation (9,000 rpm, 25 min) three times to remove excessive CTAB and dried by lyophilization.

In situ polymerization of aliphatic PUA onto Au/SiO₂ nanoparticles

DL-1-amine-2-propanol was mixed with sulfuric acid under reduced pressure distillation to form sulfate ester. After dissolving the sulfate ester solid with sodium hydroxide solution, monomer 2-methylaziridine was obtained by dry-air distillation. Then, Au/SiO₂ nanoparticles (15 mg) and 2-methylaziridine (0.6 mL) were placed in the autoclave quickly after exchanging air with pure N₂. 30 mL compressed CO₂ was injected into the reactor to pressurize continuously, and then the system was heated to 100 °C at 12.5 MPa to attach a supercritical inner environment. After stirring at 100 °C for 15 h, the reaction was stopped by taking the autoclave into an ice-water bath. The product was purified by reprecipitation from methanol/ether for three times. The dissolved aliphatic PUA in supernatant medium after in situ polymerization reaction was exacted to determine the LCST.

Characterization of Au/SiO₂/PUA nanoparticles

Transmission electron microscopy (TEM) was carried out on a Tecnai G2 20 emission electron microscope (FEI) with an accelerating voltage of 200 kV, and the copper grid was employed as the sample holder. The UV–Vis–NIR spectra of Au, Au/SiO₂, and Au/SiO₂/PUA nanoparticles and absorption of DOX were examined with ultraviolet and visible spectrophotometer (UV, Agilent Technologies Cary 5000). LCST was measured by a variable temperature mood of ultraviolet and visible spectrophotometer (UV, Agilent Technologies Cary 5000), and the wavelength number was 500 nm. Au/SiO₂/PUA nanoparticles were also measured by X-ray photoelectron spectroscopy (XPS, ESCALAB 250Xi). The zeta-potential size distribution of the nanoparticles was examined in deionized water using a Zeta-sizer (nano ZS90 Malvern Instruments), and the samples were measured three times to get average values. FTIR spectra were obtained on a BRUCK Tensor FTIR spectrometer in the range of 4000–400 cm⁻¹ using the attenuated total reflection (ATR) technique. Thermogravimetric analysis (TGA) was carried out on a TGA/DSC Thermogravimetric Analyzer (NETZSCH STA 409) with the heating rate of 10 °C min⁻¹ under an Ar atmosphere. N₂ adsorption/desorption isotherms were obtained on a Micromeritics ASAP 2020 apparatus. Brunauer–Emmett–Teller (BET) analyses were used to calculate the surface area and pore size.

DOX loading and in vitro drug release

Five milligrams of dried Au/SiO₂/PUA nanoparticles was incubated in 4 mL of DOX aqueous solution (0.5 mg mL⁻¹), and the mixer was kept at 50 °C for 1 h and another 11 h at 37 °C under gentle magnetic agitating without light. After loading DOX into nanoparticles, the solution was centrifuged by deionized water for three times to remove the unloaded DOX. The unloaded DOX amount in the supernatant was calculated via the absorption value measured by UV–Vis absorption spectroscopy at 481 nm, which employed the calibration curve of DOX. The specific DOX loading content and efficiency were calculated according to the following equations [34]:

$$\begin{aligned} \text{Drug content (mg per mg sample)} &= (\text{DOX fed} - \text{supernatant DOX}) / \\ &\quad \text{nanoparticles amount} \\ \text{DOX loading efficiency (\%)} &= (\text{DOX fed} - \text{supernatant DOX}) / \text{DOX fed} \times 100\% \end{aligned}$$

For in vitro release behavior test, centrifuged nanoparticles were dispersed into the phosphate buffer solution (PBS) with pH 7.4 or acetate buffer solution with pH 4.5 to a constant volume 1 mL in the dialysis bag. Then, the bag was merged in 11 mL blank medium at corresponding pH value and stirred in a horizontal shaker at different temperatures. The sample solution (4 mL) was extracted from release medium periodically for UV–Vis analysis and replaced by blank butter solution. For the NIR laser irradiation investigation, the same system was treated under NIR light irradiation with a wavelength centered on 808 nm at different intensity. For the NIR on–off gate investigation, the sample in the dialysis bag was irradiated over a period of 10 min and a following 5 h 50 min intervals without laser irradiation. The experiments repeated six cycles for 48 h. For thermal-responsive on/off DOX release experiment, the sample was at 55 °C over a period of 10 min and a following 5 h 50 min intervals at 37 °C. The experiments also repeated six cycles for 48 h. All the values were tested in triplicate, and the average data were shown in this study.

Cell cytotoxicity assay of Au/SiO₂/PUA

Cytotoxicity evaluation of Au/SiO₂/PUA and DOX-loaded Au/SiO₂/PUA was determined by the conventional MTT (Solarbio, Co. Ltd.) assay and microplate reader (Thermo, US). Hela cells were plated in triplicate in 96-well plates and incubated in a cell culture box at 37 °C in 5% CO₂ atmosphere for 24 h. Au/SiO₂/PUA/DOX, Au/SiO₂/PUA along, or equivalent dose of DOX was added into the wells (ranging from 0.02 to 500 µg mL⁻¹) and incubated for another 24 h. After that, 20 µL of MTT solution (5 mg mL⁻¹) was added for additional 4 h incubation. At last, 150 µL of dimethyl sulfoxide (DMSO) was used to dissolve the formazan in a low-speed shaker for 10 min, and the optical density values at 490 nm were recorded. The data were calculated into cell viability.

Results and discussion

Characterization of Au/SiO₂ and Au/SiO₂/PUA

The typical UV–Vis spectra of AuNRs, Au/SiO₂, Au/SiO₂/PUA, and Au/SiO₂/PUA/DOX were illustrated in Fig. 1. The as-prepared Au nanorods had a longitudinal surface plasmon resonance (SPR) peak at ca. 800 nm. A slight red shift (ca. 20 nm) of the SPR band between AuNRs and Au/SiO₂ was clearly observed after coating silica shell. A converse blue shift from Au/SiO₂ to Au/SiO₂/PUA could also be found in Fig. 1. This could be attributed to the local transformation on the refractive index of SiO₂ shell and PUA, respectively. Owing to the AuNRs coated by SiO₂/PUA composite shell, the clustering of nanoparticles would not influence the location of longitudinal SPR band in the NIR window. Therefore, Au/SiO₂/PUA can utilize NIR light efficiently, indicating the high potential for Au/SiO₂/PUA in the domain of epithelial therapy [22]. In addition, a slight blue shift of the band was observed after the loading of DOX. The UV–Vis absorption of Au/SiO₂/PUA/DOX also exhibited a distinct increase of DOX at 500 nm, which was overlapped with the transverse SPR band of AuNRs. Importantly, the longitudinal SPR peak of Au/SiO₂/PUA/DOX nanoparticles remained in the NIR region, which indicated that the NIR responsiveness could not be alleviated after coating the composite shell and DOX.

In the present work, we fabricated Au nanorods through conventional protocol developed by El-Sayed, which was adjusted to synthesis nanorods

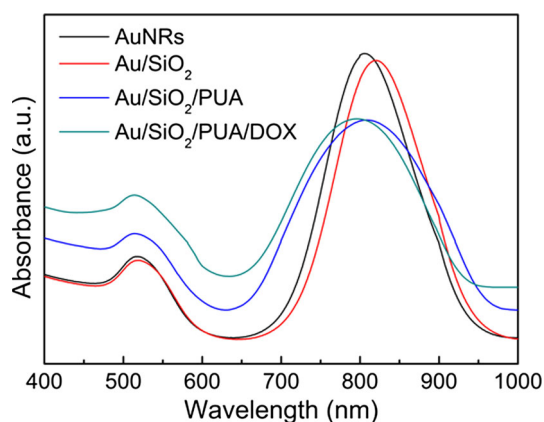


Figure 1 UV-vis spectra of AuNRs, Au/SiO₂, Au/SiO₂/PUA, and Au/SiO₂/PUA/DOX.

with specific draw ratio. The average length and width of Au nanorods in the present study were 34 ± 1.2 and 9.3 ± 0.7 nm, respectively (ca. 3.7:1 aspect ratio), as shown in Fig. 2a. The silica shell was coated by the classical method of Matsuura, which was well known to introduce mesopores over each individual AuNR core. Mesoporous silica shells of approximate 20 nm in thickness were clearly obtained (Fig. 2b).

Owing to the interaction between hydroxyl groups of silica and 2-methylaziridine, thermal-responsive PUA could be impregnated onto the surface of Au/SiO₂ nanoparticles by in situ ring-opening polymerization [35]. The structure and characterization of aliphatic PUA had been illustrated and discussed in detail in our previous report [36, 37]. Large-scale TEM images (Fig. 2c) were provided to characterize the decent monodispersity of Au/SiO₂/PUA nanoparticles. After the incorporation of PUA (Fig. 2d), the average size of Au/SiO₂/PUA was 79 ± 3.7 nm, which was slightly larger than that of Au/SiO₂ (75 ± 1.2 nm). Moreover, it could be observed from Fig. 2c and d that the porous texture of silica shell was replaced by the smooth surface morphology. The possible reason was that the porous and looser silica surface was covered by compacted aliphatic PUA polymer chain. Size distribution analysis of Au/SiO₂ and Au/SiO₂/PUA nanoparticles measured from Zeta-sizer is presented in Figure S2†. Au/SiO₂ and Au/SiO₂/PUA nanoparticles were uniform in a narrow distribution with diameters of around 60 nm and 100 nm. It should be noted that the diameter of Au/SiO₂/PUA measured from Zeta-sizer (100 nm) was larger than that calculated from TEM image (79 nm). The possible reason to this phenomenon is the slight aggregation of Au/SiO₂/PUA nanoparticles after the incorporation of PUA. The zeta-potential of Au/SiO₂ was -9.8 ± 0.4 mV while the value for Au/SiO₂/PUA was 18.8 ± 0.6 mV, indicating the incorporation of strongly electropositive PUA onto the silica shell.

Figure 3a presents the FTIR spectra of Au/SiO₂ and Au/SiO₂/PUA nanoparticles, which could also provide clear evidence for the successful grafting of aliphatic PUA onto silica shell. For both nanoparticles, the characteristic peaks of SiO₂ were detected at 1061, 450, and 811 cm⁻¹, which generally assigned to the stretching and rocking vibrations of Si–O–Si and bending vibrations of O–Si–O, respectively. Compared with Au/SiO₂ nanoparticles, it was obvious

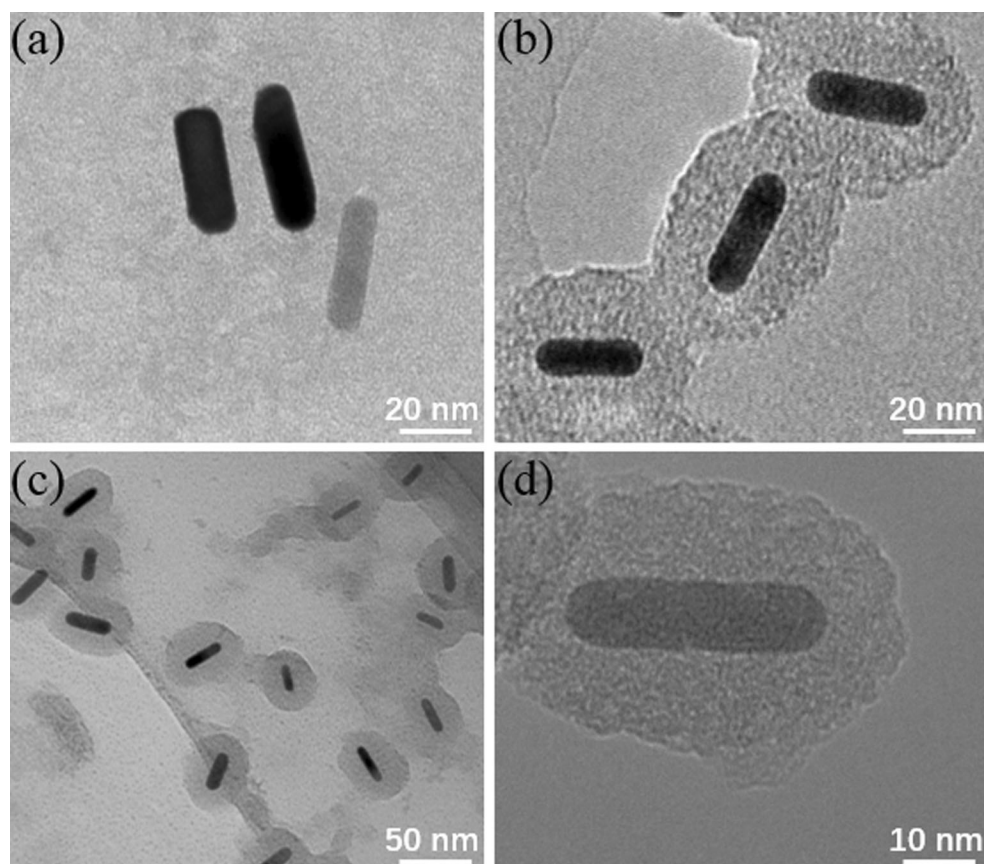


Figure 2 TEM images of AuNRs (a), Au/SiO₂ (b), and Au/SiO₂/PUA (c and d).

that characteristic absorbance peaks of PUA could be observed. The new absorption peak at 2370 cm^{-1} was assigned to the in situ CO₂ reaction condition, the peak at 1700 cm^{-1} could be attributed to the stretching vibration of C=O, and another peak at 1217 cm^{-1} belonged to stretching vibration of C–O [38]. Thermogravimetric analysis curves of the Au/SiO₂ and Au/SiO₂/PUA nanoparticles are shown in Fig. 3b. Both samples showed weight losses below 150 °C that resulted from the physical loss of water. In the range of 200–500 °C, a remarkable weight loss (17.81%) of Au/SiO₂/PUA nanoparticles could be attributed to the polymer decomposition, indicating that the grafted-PUA content in hybrid nanoparticles was around 17.81% in weight. The nitrogen adsorption–desorption isotherms of Au/SiO₂ and Au/SiO₂/PUA nanoparticles exhibited type IV curves (Fig. 3c). Au/SiO₂ had a Brunauer–Emmett–Teller (BET) surface area of $51.33\text{ m}^2\text{g}^{-1}$ and a BJH pore diameter of 1.13 nm (Fig. 3d). After coating with PUA, Au/SiO₂/PUA nanoparticles had a BET surface area of $337.49\text{ m}^2\text{g}^{-1}$ and a BJH pore diameter of 1.03 nm.

The large specific surface area enabled Au/SiO₂/PUA nanoparticles to be suitable for a high drug-loading efficiency, which was vital for remotely controllable drug delivery vehicles.

To further understand the successful grafting of PUA onto the surface of Au/SiO₂ nanoparticles, the results of X-ray photoelectron spectroscopy (XPS) were also exhibited. Figure 4a and 4b shows the high-resolution spectra of ungrafted Au/SiO₂ and Au/SiO₂/PUA nanoparticles on the domain of C 1s multiplex scans. Both the curves were decomposed into Gaussian peaks by using a classical curve-fitting procedure. Firstly, it was obvious that Au/SiO₂ and Au/SiO₂/PUA nanoparticles possessed three and five separate peaks, respectively. Two new peaks at 287.7 and 285.5 eV for Au/SiO₂/PUA nanoparticles were attributed to C=O and C–N species derived from grafted aliphatic PUA. XPS results further confirmed that PUA had been successfully grafted onto the mesoporous silica shells.

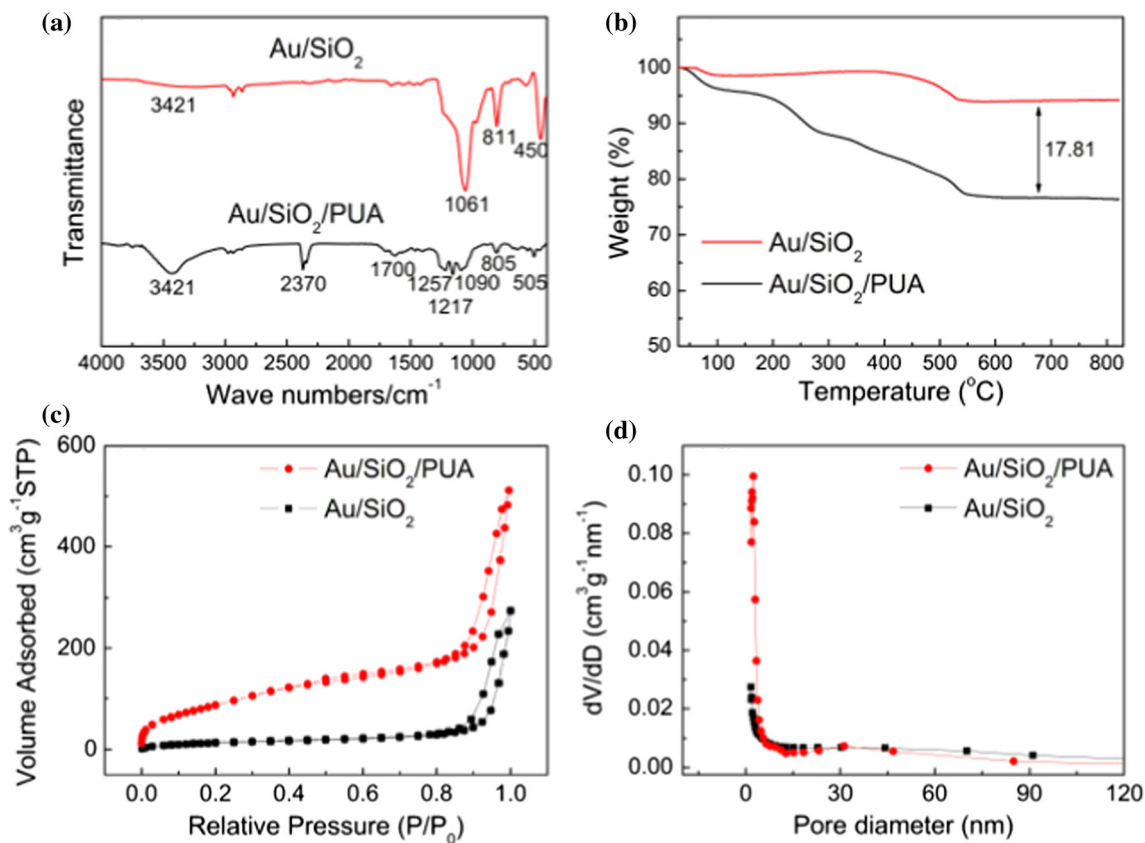


Figure 3 FTIR spectra (a) and TGA curves (b) of Au/SiO₂ and Au/SiO₂/PUA; N₂ adsorption–desorption isotherms (c) and pore size distributions (d) of Au/SiO₂ and Au/SiO₂/PUA.

In vitro photothermal transition properties

In the present research, we combined Au nanorods and aliphatic PUA to be an intelligent drug delivery vehicle. AuNRs inside the Au/SiO₂/PUA provided a powerful mode of confining light to metal/dielectric interfaces, and it also in turn converted the laser light into ambient heat with an intense local electromagnetic fields. Furthermore, whether the ambient temperature could attach even exceed the LCST of PUA was a critical issue in the present study.

Prior to applying NIR light to activate the external heating-triggered drug release, the NIR light-induced temperature variety of Au/SiO₂/PUA suspension in PBS solution was recorded first [39, 40]. To better understand the effect of PUA layer on the photothermal transition efficiency of Au/SiO₂ nanoparticles, the temperature images of nanoparticles suspension under NIR laser irradiation at 1, 2, and 4 W/cm² were recorded by an IR camera, as shown in Fig. 4c. Au/SiO₂/PUA nanoparticles were irradiated by NIR laser at its longitudinal SPR wavelength,

which was considered the insufficient absorption of NIR light under unmatched wavelengths [41]. The temperature of Au/SiO₂/PUA nanoparticle suspension increased rapidly and eventually reached a plateau in the focal region within 10 min, and corresponding infrared thermogram (Fig. 4c) illustrated the accurate interaction between the temperature of Au/SiO₂/PUA suspension and NIR laser intensity.

On the other hand, the heating up (ΔT) within 60 min of the Au/SiO₂/PUA suspension was recorded under different laser power densities, as shown in Fig. 4d. The temperature of Au/SiO₂/PUA suspension increased to around 39, 54, and 80 °C under NIR irradiation at 1, 2, and 4 W/cm², respectively. The distinct temperature decrease was perhaps derived from the dramatic reshaping of AuNRs from rodlike to sphere upon NIR irradiation. The poor shape stability of was consistent with the absorbance decrease of UV–Vis–NIR spectra, which could weaken the photothermal conversion efficiency of Au/SiO₂ nanoparticles. When the NIR laser intensity was over 2 W/cm², the environment temperature

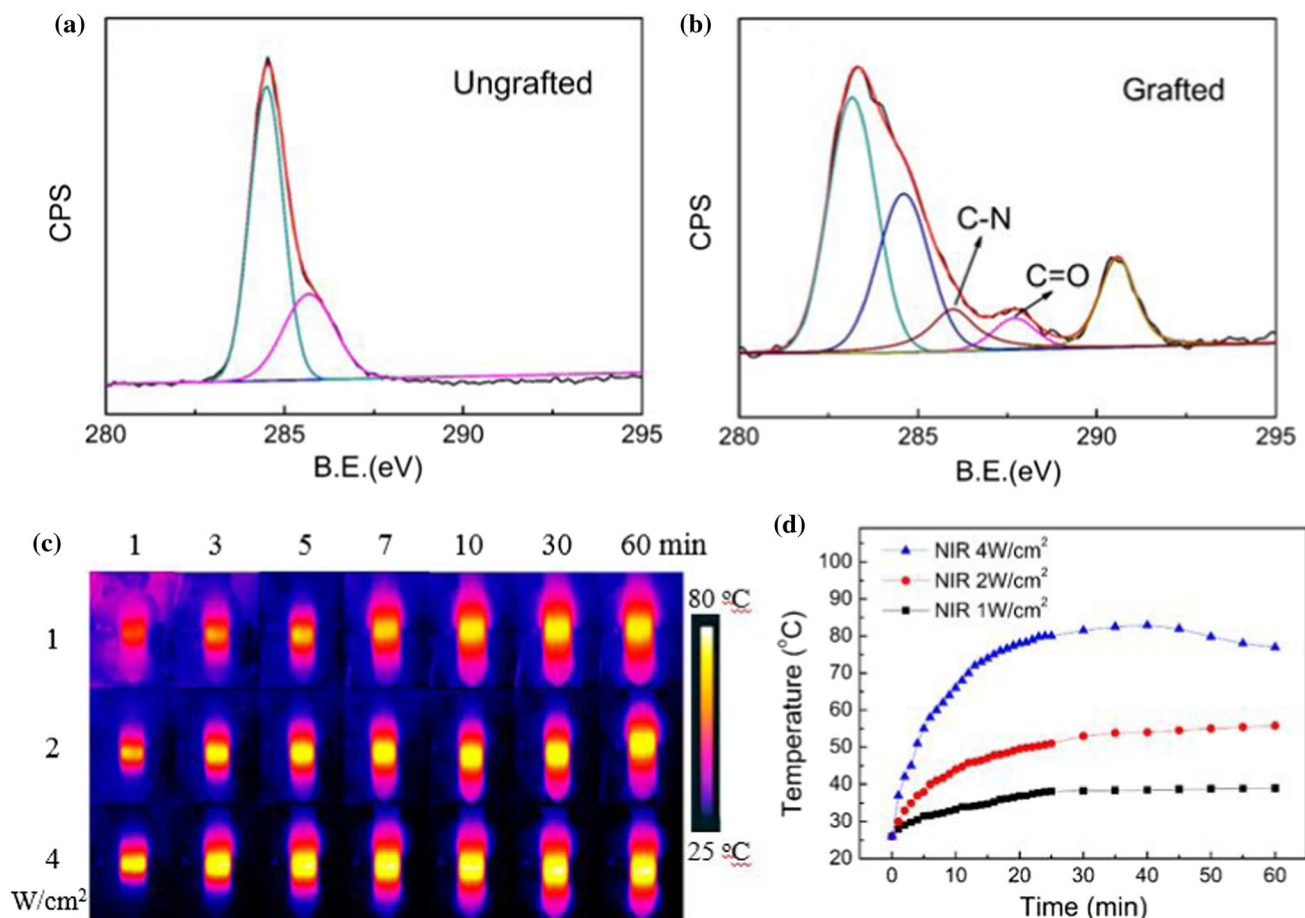


Figure 4 High-resolution XPS spectra of C1s region of Au/SiO₂ (a) and Au/SiO₂/PUA (b); the temperature images of nanocomposite suspension under NIR laser (808 nm) irradiation recorded

by an IR camera at different laser intensity (c); The temperature variation of Au/SiO₂/PUA suspension upon different intensity of NIR laser irradiation (d).

generated by nanoparticles met the LCST of aliphatic PUA. As revealed in previous reports [42], the local temperature at the surface of the heating generators was higher than the apparent temperature of the aqueous dispersion. For example, even though the human body temperature was below the LCST of the PUA, the switching temperature could be easily achieved by increasing the intensity of NIR light. These results indicated that the irradiation intensity and exposure time dominated the temperature of nanoparticle suspension. Therefore, it could be expected that Au/SiO₂/PUA nanocomposites had significant potential as a light-responsive release system, which triggers the release of the loaded drug with the NIR-sensitive AuNRs and thermo-sensitive PUA.

As demonstrated by a temperature-variable UV-Vis spectrometer, the LCST of aliphatic PUA was 54 °C (Fig. 5a). ¹H NMR and ¹³C NMR of aliphatic

PUA in Figure S3† had demonstrated the chemical structure of aliphatic PUA [43]. The polymers consist of hydrophobic urethane and hydrophilic amine and exhibit a good thermally induced reversible transition property in aqueous solution. As a main driving force, the hydrogen bonds between amino groups and water are advantageous to the polymeric dissolution in water. As the temperature increased, the H-bond-assisted hydrophilicity is counterbalanced by the increased hydrophobicity owing to the fractional breakdown of hydrogen bonds, which will lead to a spontaneous macromolecular aggregation [44].

Figure 5b illustrates gate-responsive release mechanism of Au/SiO₂/PUA nanoparticles. The PUA chains were swollen when the temperature was below the LCST of PUA. The mesoporous silica shells were covered by the stretched PUA polymeric chains, resulting in the little drug release. In contrast, the mesopores of Au/SiO₂ nanoparticles were opened

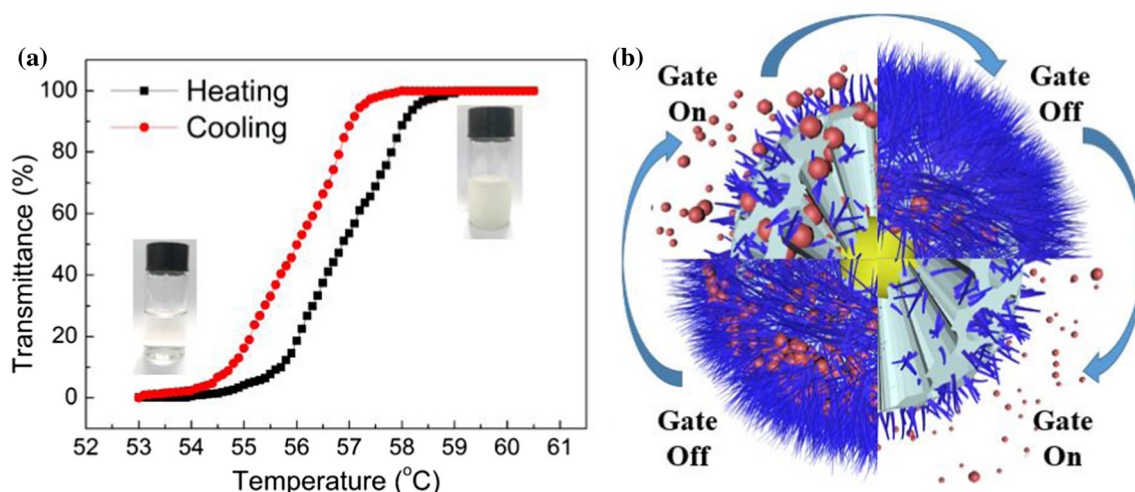


Figure 5 Plots of transmittance as a function of temperature measured for aqueous solution of aliphatic PUA (2.0 wt %) (a); Gate-responsive release mechanism of Au/SiO₂/PUA nanoparticles (b).

because of the shrinkage of PUA when the temperature was above the LCST, which resulted in the fast drug release. When the temperature decreased below the LCST, the PUA chains stretched and drug release paused again. This thermal-dependent “on/off” characteristics enabled the drug release in a controlled way by simply adjusting the environmental temperature. As we revealed, the environment temperature would increase quickly when the NIR-responsive nanoparticles were irradiated by NIR light. Therefore, it could be expected that the thermal “on/off gate” within Au/SiO₂/PUA nanoparticles could be simply adjusted by NIR irradiation in the present study.

DOX loading and thermal/pH-responsive drug release

Au/SiO₂/PUA nanoparticles with a mesoporous silica and polymer shell have a great potential as an excellent drug-loading vehicle. The DOX efficiency of Au/SiO₂/PUA was calculated to be about $35.86 \pm 2.3\%$, and the drug content was approximately 0.55 ± 0.007 mg per 10 mg sample [45]. Figure 6a shows the in vitro release curves of Au/SiO₂/PUA nanoparticles, which are attributed to the temperature-dependent release properties of PUA. The LCST of aliphatic PUA employed in the present study was 54 °C. Therefore, 37 and 55 °C were selected as the temperature conditions to study the influence of temperatures below and above LCST on

the release behavior [46]. At 37 °C, the drug release was only 1.40% over the initial 1 h due to the blocking effect of the loose polymer chains in the mesopores of silica shells. In contrast, about 6.54% loaded drug was released within 1 h at 55 °C, which may be caused by the rapid shrinkage of polymer chains. Moreover, the drug release was 16.6% at 55 °C over 24 h, which was almost two times as that at 37 °C. Student’s *t* test analysis showed that the difference between the release of Au/SiO₂/PUA nanoparticles at 55 and 37 °C was extremely statistically significant (*p* value was 0.0001, greater than 99% confidence).

The in vitro release curves of Au/SiO₂/PUA nanoparticles in response to pH changes are shown in Fig. 6b. In the present study, we chose phosphate buffer solution (PBS) with pH 7.4 as the standard medium. Acetate buffer solution with pH 4.5 was employed as the contrast pH condition to stimulate the acid environment in tumor. It could be observed that the DOX release increased when pH value decreased from 7.4 to 4.5. Only 6.77% of DOX was released at pH 7.4 over 24 h, but 15.12% of DOX was released at pH 4.5 for the same period. The rapid release of Au/SiO₂/PUA nanoparticles at pH 4.5 was partly due to the alleviated hydrogen-bond interaction between DOX and silica in the acidic solution [10]. The *p* value obtained from Student’s test analysis in the comparison between the release at pH 7.4 and 4.5 was less than 0.0001.

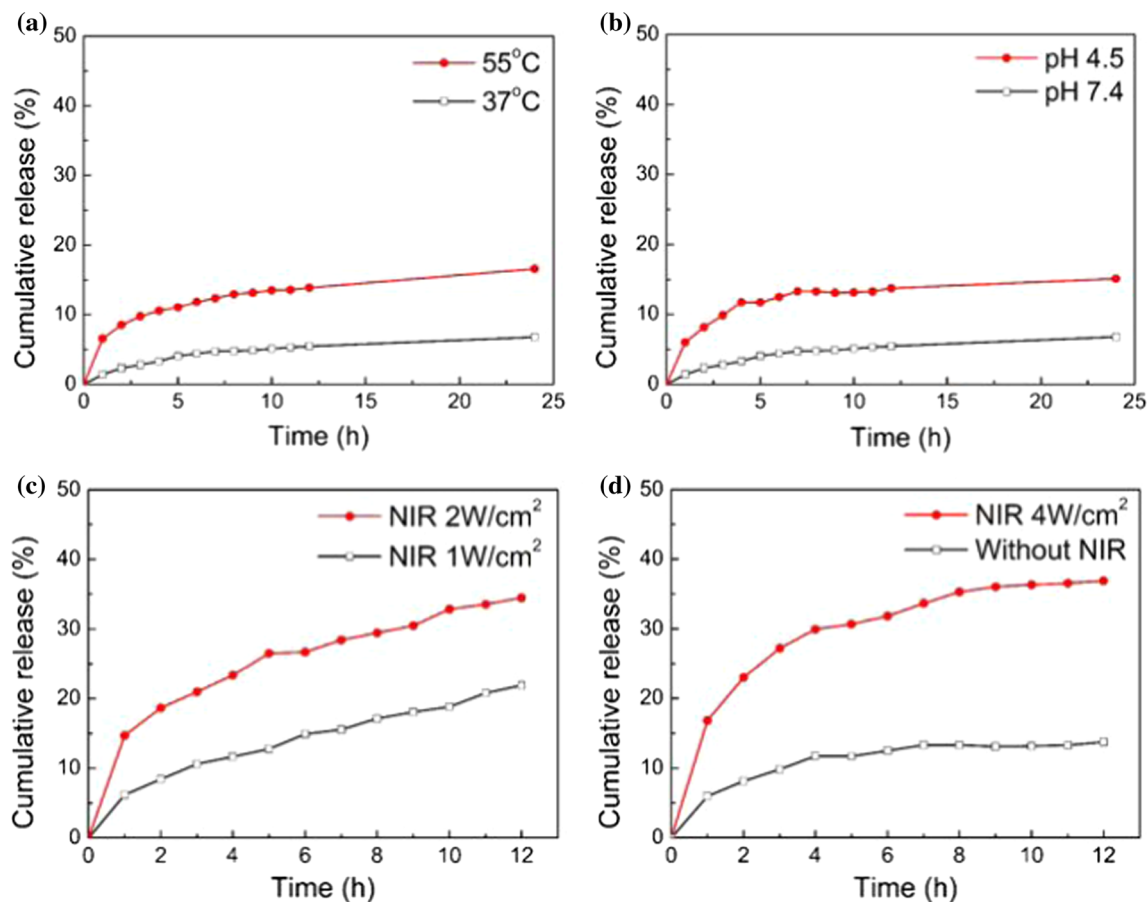


Figure 6 Thermal-dependent release profiles of Au/SiO₂/PUA nanoparticles at pH 7.4 (a); pH-responsive drug release of Au/SiO₂/PUA nanoparticles at 37 °C (b); DOX release profiles of Au/SiO₂/PUA

at different laser intensities at pH 7.4 and 37 °C (c); DOX release profiles with or without NIR irradiation at pH 4.5 and 37 °C (d).

NIR-responsive drug release

AuNRs were well known for transforming NIR light to local heat, which could be applied in selective treatment of solid tumors. A CW diode laser with a center wavelength of 808 nm was utilized to investigate the NIR-responsive DOX release of Au/SiO₂/PUA nanoparticles. The release behaviors under different NIR laser power (1 and 2 W/cm²) in weak basic solution (pH 7.4) are shown in Fig. 6c. The cumulative DOX release reached to 21.86 and 34.47%, respectively, upon the exposure to different NIR laser irradiation for 12 h. However, only 5.45% of DOX was released from Au/SiO₂/PUA nanoparticles without NIR irradiation as illustrated in Fig. 6a. Obviously, the triggered rapid drug release upon NIR irradiation could be ascribed to the high ambient temperature generated by AuNRs under high level of

laser intensity, which facilitated the fast DOX release of the nanoparticles.

We also compared the NIR-responsive behavior under acidic environment. It should be noted from Fig. 6d that the cumulative DOX release reached to 36.85% upon NIR laser irradiation for 12 h at pH 4.5, which was significantly higher than that without NIR irradiation (15.12%). The drug release rate could be significantly enhanced by laser irradiation in acidic medium because the laser-converted heat [47] could efficiently dissociate the electrostatic interaction between DOX and the polymer shell at pH 4.5. Student's *t* test analysis indicated that the DOX release of Au/SiO₂/PUA with different laser intensity and pH values were extremely statically significant (the *p* values were both less than 0.0001, greater than 99% confidence).

Reversible drug release

The main reason for the rapid release of Au/SiO₂/PUA hybrid nanoparticles at high intensity of laser irradiation was the shrinkage of PUA above its LCST, which introduced “on/off gate” effect in this hybrid drug carrier. Instead of precipitating from the nanoparticle bulk, the shrinkage of PUA in the present design would not break the intact structure of Au/SiO₂ nanoparticles because PUA chains were mostly attached on the surface of mesoporous silica [25]. Therefore, it was also anticipated the better NIR reversibility could be realized by Au/SiO₂/PUA nanoparticles under alternate NIR light irradiation for the sake of the excellent thermal-responsive effect of aliphatic PUA.

To confirm this assumption, the Au/SiO₂/PUA nanoparticles were treated by alternating temperatures between 37 and 55 °C, or with NIR laser on/off alternating treatment at pH 7.4 and pH 4.5, respectively. In this experiment, Au/SiO₂/PUA nanoparticles were treated for the first 10 min under laser irradiation or at 55 °C, and then the laser irradiation was removed or the samples were moved to the medium of 37 °C for following 5 h 50 min [1]. Both drug release experiments with temperature/NIR alternating were performed six circles for 48 h, and then the drug release profiles were obtained as described in Fig. 7. A clear stair-like release pattern could be clearly observed. The drug release values for first circle were 3.43% and 6.31% at pH 7.4, while the final amount of DOX release reached to 10.58 and 15.35%, respectively (Fig. 7a). It could also be noted

that the reversible release property at pH 4.5 (Fig. 7b) was more distinct than that at pH 4.5 (Fig. 6a). The possible reason for this phenomenon is that the hydrogen-band interaction between DOX and silica in the acidic medium is alleviated, resulting in the relatively rapid DOX release.

It was notable that the “on/off gate” effect was more obvious under the laser irradiation condition rather than external heating as discussed above, owing to the relative higher local temperature generated by AuNRs core [22]. The above results demonstrated that a remote NIR light could be employed to activate the phase change and subsequent drug release of Au/SiO₂/PUA hybrid nanoparticles. The polymeric on/off transition introduced a distinct stairs-like DOX release behavior by simply adjusting the on/off of laser irradiation, which had a great potential to be employed as a remote controllable drug carrier.

Biocompatibility and cell cytotoxicity

The results of cell cytotoxicity evaluation of Au/SiO₂/PUA, Au/SiO₂/PUA-DOX, and DOX are illustrated in Fig. 8a. It was obvious that Au/SiO₂/PUA nanoparticles without DOX loading exhibited a relatively good biocompatibility at a wide range of concentrations. Pretty low cytotoxicity was quite reasonable since all the main constituents of Au/SiO₂/PUA nanoparticles as a drug carrier had previously proven to be of low bio-toxicity and favorable biocompatibility [10, 26]. The cell lines also demonstrated that potential toxic substance, such as CTAB,

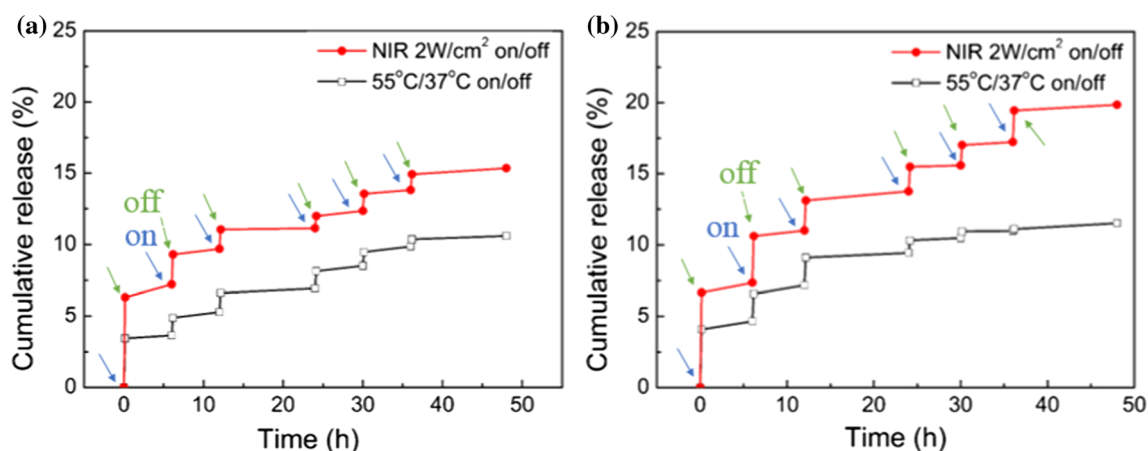


Figure 7 DOX release profiles of Au/SiO₂/PUA under alternating heating sequences and NIR laser irradiation sequences (808 nm, 2 W/cm²) at pH 7.4 (a) and pH 4.5 (b).

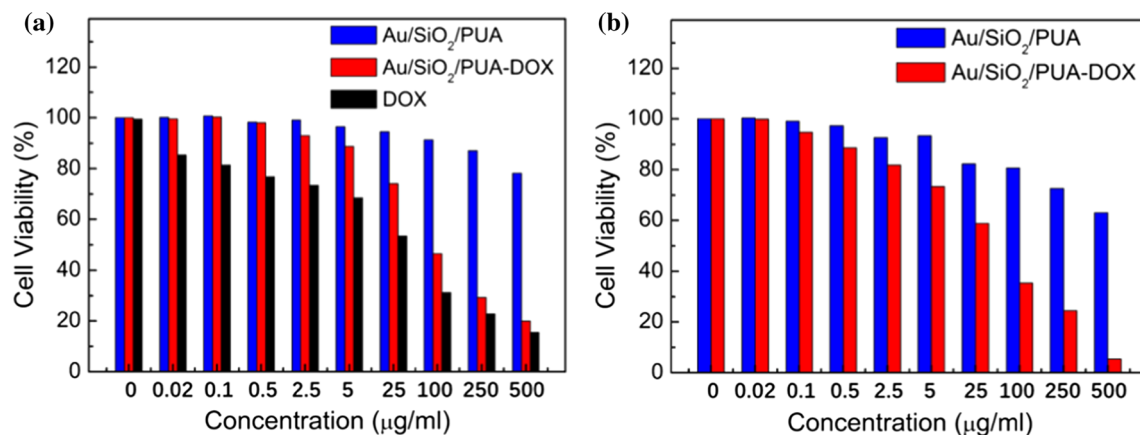


Figure 8 Cytotoxicity evaluation of Au/SiO₂/PUA, Au/SiO₂/PUA-DOX, and DOX (a); Cytotoxicity evaluation of Au/SiO₂/PUA, Au/SiO₂/PUA-DOX after laser irradiation (808 nm, 2 W/cm²) (b).

TEOS, and methanol used in the synthesis of Au/SiO₂/PUA nanoparticles, had been removed during the purification process.

Secondly, it was well known that the free DOX in the human body had a great poisonousness and many severe side effects, such as cardiac failure, haematopoiesis dysfunction, and serious hepatic function damage. The gate effect of Au/SiO₂/PUA at pH 7.4 and human body temperature would restrain large release of DOX during in vivo circulation and then reduce various side effects and cytotoxicity for normal tissues. And DOX-loaded Au/SiO₂/PUA also exhibited higher cytotoxicity on Hela cells than unloaded Au/SiO₂/PUA did, which could be attributed to partial release of DOX in acid tumor [48] environment.

In order to explore the photothermal therapeutic effect of Au/SiO₂/PUA and Au/SiO₂/PUA-DOX, the cell viability after NIR light treatments (808 nm, 2 W/cm²) was measured by MTT viability assays, as shown in Fig. 8b. The Au/SiO₂/PUA upon NIR irradiation showed the relatively high photothermal therapy efficiency, and 36.99% of the cells were killed at a sample concentration of 500 μg/mL because of the photothermal effect of AuNRs. It could also be found from Fig. 8b that Au/SiO₂/PUA-DOX (500 μg/mL) almost all of the cells (94.59%) were killed, indicating the significant chemophotothermal synergistic therapy effect of Au/SiO₂/PUA-DOX upon NIR irradiation.

Drug release kinetics

The cumulative release and time had been fitted to the following empirical equation (Rigter–Peppas release model) to analyze the kinetics of DOX release process of Au/SiO₂/PUA:

$$M_t/M_\infty = kt^n \quad (1)$$

In this conventional model, M_t is the cumulative amount of released DOX at any time t ; M_∞ is the total amount of loaded DOX in the nanoparticles; k is the release constant relating to the structures and properties of nanoparticles; and n is the diffusion exponent characterizing difference in the specific release mechanism.

The specific DOX release kinetics of Au/SiO₂/PUA in different experimental conditions were analyzed, and Table S1† exhibited the figures for k , n , and correlation coefficient (R^2). Figure S4† shows the curves of $\ln(M_t/M_\infty)$ versus $\ln t$ for Au/SiO₂/PUA at different temperatures, pH values, and NIR irradiation intensities. As discussed in other paper [34], Figure S4a† shows the curves of $\ln(M_t/M_\infty)$ versus $\ln t$ for Au/SiO₂/PUA nanoparticles in the neutral PBS at 37 and 55 °C. The n values of Au/SiO₂/PUA ranged from 0.7160 to 0.2998 and produced a shift from Case II transport to Fickian diffusion at 37 °C. At the 55 °C, the Au/SiO₂/PUA had the n values ranging from 1 to 0.3226, indicating a shift from super Case II diffusion to Fickian diffusion. This may be due to the grafting of PUA chains which exhibited change from hydrophilia to hydrophobicity [25]. Owing to transition of PUA, the release pattern of Au/SiO₂/PUA

nanoparticles had a rapid transfer. Figure S4b† illustrates that n value of Au/SiO₂/PUA at pH 4.5 and 37 °C experienced a similar shift compared with release behavior in the pH 7.4 environment, which shifted from 0.6138 to 0.2323. This phenomenon may be attributed to that pH only changes the interactions between DOX and matrix rather than changing the structure and property of the nanoparticles. The results demonstrated indirectly the totally different release pattern below and above the LCST and biostability in acid environment, which exerted a significant influence on the temperature-responsive drug release behavior of hybrid nanoparticles.

Figure S4c and S4d† showed the curves of $\ln(M_t/M_\infty)$ plot versus $\ln t$ for Au/SiO₂/PUA with different intensity of NIR laser irradiation. On the one hand, it was obvious that different NIR irradiation changed the release behavior rapidly, which shifted from 1 to 0.4888 and 0.3474, respectively [38]. Furthermore, it was observed that release pattern of Au/SiO₂/PUA under 2 W/cm² laser irradiation was more corresponded to it at 55 °C, which was also related to the heat generated by AuNRs cores when they were irradiated under acute NIR light. On the other hand, the n value of Au/SiO₂/PUA with laser irradiation at pH 4.5, which ranged from 1 to 0.3368, indicated a shift from super Case II diffusion to non-Fickian diffusion or anomalous diffusion, while NIR irradiation changed the diffusion mode by heating the Au/SiO₂/PUA nanoparticles. These phenomena demonstrate indirectly that AuNRs could effectively convert NIR light into heat, heat switch on the polymer gate, and then enhance the drug delivery rate of Au/SiO₂/PUA remarkably.

Conclusion

In conclusion, a novel multi-responsive drug deliver carrier was fabricated by grafting the thermal-/pH-responsive aliphatic PUA onto Au/SiO₂ nanoparticles via in situ polymerization under supercritical CO₂. The in vitro drug release studies indicated that Au/SiO₂/PUA nanoparticles exhibited distinguishable pH-, thermal-, and near-infrared (NIR)-dependent drug release properties. In addition, Au/SiO₂/PUA nanoparticles combined the NIR light-heat conversion property of AuNRs with the thermal sensitivity of PUA to build an on/off drug release gate controlled by remote laser irradiation. The on/

off gate effect of AuNRs/PUA introduced a distinct stairs-like DOX release behavior by adjusting the on/off of laser irradiation. The present paper provides a facile and green route to fabricate smart hierarchical nanoparticles by combining intelligent polymer, mesoporous silica, and Au nanorods, which shows great potential in controllable drug delivery area.

Acknowledgements

This work was financially supported by Henan Provincial Natural Science Foundation of China (Project No. 162300410257) and National Natural Science Foundation of China (Project No. 20874090).

Electronic supplementary material: The online version of this article (<https://doi.org/10.1007/s10853-018-2117-7>) contains supplementary material, which is available to authorized users.

References

- [1] Liu J, Detrembleur C, De Pauw-Gillet MC, Mornet S, Jerome C, Duguet E (2015) Gold nanorods coated with mesoporous silica shell as drug delivery system for remote near infrared light-activated release and potential phototherapy. *Small* 11:2323–2332
- [2] Mura S, Nicolas J, Couvreur P (2013) Stimuli-responsive nanocarriers for drug delivery. *Nat Mater* 12:991–1003
- [3] Brigger I, Dubernet C, Couvreur P (2012) Nanoparticles in cancer therapy and diagnosis. *Adv Drug Deliv Rev* 64:24–36
- [4] Chávez G, Campos CH, Jiménez VA, Torres CC, Díaz C, Salas G, Guzmán L, Alderete JB (2017) Polyamido amine (PAMAM)-grafted magnetic nanotubes as emerging platforms for the delivery and sustained release of silibinin. *J Mater Sci* 52:9269–9281. <https://doi.org/10.1007/s10853-017-1140-4>
- [5] Chen Y, Zhang ZH, Han X, Yin J, Wu ZQ (2016) Oxidation and acid milieu-disintegratable nanovectors with rapid cell-penetrating helical polymer chains for programmed drug release and synergistic chemo-photothermal therapy. *Macromolecules* 49:7718–7727
- [6] Rai P, Mallidi S, Zheng X, Rahmzadeh R, Mir Y, Elrington S, Khurshid A, Hasan T (2010) Development and applications of photo-triggered theranostic agents. *Adv Drug Deliv Rev* 62:1094–1124
- [7] Xie J, Lee S, Chen X (2010) Nanoparticle-based theranostic agents. *Adv Drug Deliv Rev* 62:1064–1079

- [8] Fang L, Wang W, Liu Y, Xie Z, Chen L (2017) Janus nanostructures formed by mesoporous silica coating Au nanorods for near-infrared chemo-photothermal therapy. *J Mater Chem B* 5:8833–8838
- [9] Shen S, Tang H, Zhang X, Ren J, Pang Z, Wang D, Gao H, Qian Y, Jiang X, Yang W (2013) Targeting mesoporous silica-encapsulated gold nanorods for chemo-photothermal therapy with near-infrared radiation. *Biomaterials* 34:3150–3158
- [10] Zhang Z, Wang L, Wang J, Jiang X, Li X, Hu Z, Ji Y, Wu X, Chen C (2012) Mesoporous silica-coated gold nanorods as a light-mediated multifunctional theranostic platform for cancer treatment. *Adv Mater* 24:1418–1423
- [11] Tang F, Li L, Chen D (2012) Mesoporous silica nanoparticles: synthesis, biocompatibility and drug delivery. *Adv Mater* 24:1504–1534
- [12] Wang Y, Shi W, Wang S, Li C, Qian M, Chen J, Huang R (2016) Facile incorporation of dispersed fluorescent carbon nanodots into mesoporous silica nanosphere for pH-triggered drug delivery and imaging. *Carbon* 108:146–153
- [13] Chu Z, Yin C, Zhang S, Lin G, Li Q (2013) Surface plasmon enhanced drug efficacy using core-shell Au@SiO₂ nanoparticle carrier. *Nanoscale* 5:3406–3411
- [14] Coll C, Bernardos A, Martínezmã ÆER, SancenãN F (2013) Gated silica mesoporous supports for controlled release and signaling applications. *Acc Chem Res* 46:339–349
- [15] Baek S, Singh RK, Kim TH, Seo JW, Shin US, Chrzanowski W, Kim HW (2016) Triple hit with drug carriers: pH- and temperature- responsive theranostics for multimodal chemo- and photothermal therapy and diagnostic applications. *ACS Appl Mater Interfaces* 8:8967–8979
- [16] Chen X, Soeriyadi AH, Lu X, Sagnella SM, Kavallaris M, Gooding JJ (2014) Dual bioresponsive mesoporous silica nanocarrier as an “AND” logic gate for targeted drug delivery cancer cells. *Adv Funct Mater* 24:6999–7006
- [17] Tarn D, Ashley CE, Xue M, Carnes EC, Zink JI, Brinker CJ (2013) Mesoporous silica nanoparticle nanocarriers: bio-functionality and biocompatibility. *Acc Chem Res* 46:792–801
- [18] Zhu CL, Lu CH, Song XY, Yang HH, Wang XR (2011) Bioresponsive controlled release using mesoporous silica nanoparticles capped with aptamer-based molecular gate. *J Am Chem Soc* 133:1278–1281
- [19] Yang X, Liu X, Liu Z, Pu F, Ren J, Qu X (2012) Near-infrared light-triggered, targeted drug delivery to cancer cells by aptamer gated nanovehicles. *Adv Mater* 24:2890–2895
- [20] Singh N, Karambelkar A, Gu L, Lin K, Miller JS, Chen CS, Sailor MJ, Bhatia SN (2011) Bioresponsive mesoporous silica nanoparticles for triggered drug release. *J Am Chem Soc* 133:19582–19585
- [21] Sobot D, Mura S, Yesylevskyy SO, Dalbin L, Cayre F, Bort G, Mougín J, Desmaële D, Lepetremouelhi S, Pieters G (2017) Conjugation of squalene to gemcitabine as unique approach exploiting endogenous lipoproteins for drug delivery. *Nat Comm* 8:1–9
- [22] Zhang Z, Wang J, Nie X, Wen T, Ji Y, Wu X, Zhao Y, Chen C (2014) Near infrared laser-induced targeted cancer therapy using thermoresponsive polymer encapsulated gold nanorods. *J Am Chem Soc* 136:7317–7326
- [23] Xu X, Bai B, Wang H, Suo Y (2017) A near-infrared and temperature-responsive pesticide release platform through core-shell polydopamine@PNIPAm nanocomposites. *ACS Appl Mater Interfaces* 9:6424–6432
- [24] Pester CW, Konradi A, Varnholt B, Van Rijn P, Böker A (2012) Microstructures: responsive macroscopic materials from self-assembled cross-linked SiO₂- PNIPAAm core/shell structures. *Adv Funct Mater* 22:1723
- [25] Wu Q, Shi J, Wei J, Yang L, Cao S (2015) *In situ* functionalization of hollow mesoporous hydroxyapatite with thermal-responsive on-off gates in supercritical CO₂. *RSC Adv* 5:70101–70108
- [26] Zdrahala RJ, Zdrahala IJ (1999) Biomedical applications of polyurethanes: a review of past promises, present realities, and a vibrant future. *J Biomater Appl* 14:67–90
- [27] Alkilany AM, Thompson LB, Boulos SP, Sisco PN, Murphy CJ (2012) Gold nanorods: their potential for photothermal therapeutics and drug delivery, tempered by the complexity of their biological interactions. *Adv Drug Deliv Rev* 64:190–199
- [28] An X, Zhan F, Zhu Y (2013) Smart photothermal-triggered bilayer phase transition in AuNPs-liposomes to release drug. *Langmuir* 29:1061–1068
- [29] Boisselier E, Astruc D (2009) Gold nanoparticles in nanomedicine: preparations, imaging, diagnostics, therapies and toxicity. *Chem Soc Rev* 38:1759–1782
- [30] He Q, Shi J (2011) Mesoporous silica nanoparticle based nano drug delivery systems: synthesis, controlled drug release and delivery, pharmacokinetics and biocompatibility. *J Mater Chem* 21:5845–5855
- [31] Lee CH, Cheng SH, Wang YJ, Chen YC, Chen NT, Souris J, Chen CT, Mou CY, Yang CS, Lo LW (2009) Near-infrared mesoporous silica nanoparticles for optical imaging: characterization and in vivo biodistribution. *Adv Funct Mater* 19:215–222
- [32] And BN, Elsayed MA (2003) Preparation and growth mechanism of gold nanorods (NRs) using seed-mediated growth method. *Chem Mater* 15:1957–1962
- [33] Gorelikov I, Matsuura N (2008) Single-step coating of mesoporous silica on cetyltrimethyl ammonium bromide-capped nanoparticles. *Nano Lett* 8:369–373

- [34] Wei J, Shi J, Wu Q, Yang L, Cao S (2015) Hollow hydroxyapatite/polyelectrolyte hybrid microparticles with controllable size, wall thickness and drug delivery properties. *J Mater Chem B* 3:8162–8169
- [35] Pezaranguren PL, Vega LF, Domingo C (2013) A new method using compressed CO₂ for the in situ functionalization of mesoporous silica with hyperbranched polymers. *Chem Commun* 49:11776–11779
- [36] Ihata O, Kayaki Y, Ikariya T (2004) Synthesis of thermoresponsive polyurethane from 2-methylaziridine and supercritical carbon dioxide. *Angew Chem* 43:717–719
- [37] And OI, Kayaki Y, Ikariya T (2005) Aliphatic poly(urethane-amine)s synthesized by copolymerization of aziridines and supercritical carbon dioxide. *Macromolecules* 38:6429–6434
- [38] Xu S, Shi J, Feng D, Yang L, Cao S (2014) Hollow hierarchical hydroxyapatite/Au/polyelectrolyte hybrid microparticles for multi-responsive drug delivery. *J Mater Chem B* 2:6500–6507
- [39] Zhang Z, Shi J, Song Z, Zhu X, Zhu Y, Cao S (2018) A synergistically enhanced photothermal transition effect from mesoporous silica nanoparticles with gold nanorods wrapped in reduced graphene oxide. *J Mater Sci* 53:1810–1823. <https://doi.org/10.1007/s10853-017-1628-y>
- [40] Sun Q, You Q, Pang X, Tan X, Wang J, Liu L, Guo F, Tan F, Li N (2017) A photoresponsive and rod-shape nanocarrier: single wavelength of light triggered photothermal and photodynamic therapy based on AuNRs-capped & Ce6-doped mesoporous silica nanorods. *Biomaterials* 122:188–200
- [41] Liu J, Detrembleur C, Hurtgen M, Debuigne A, Pauw-gillet MCD, Mornet S, Duguet E, Jérôme C (2013) Reversibly crosslinked thermo- and redox-responsive nanogels for controlled drug release. *Polym Chem* 5:77–88
- [42] Liu J, Detrembleur C, Debuigne A, Pauw-gillet MCD, Mornet S, Elst LV, Laurent S, Duguet E, Jérôme C (2014) Glucose-, pH- and thermo-responsive nanogels crosslinked by functional superparamagnetic maghemite nanoparticles as innovative drug delivery systems. *J Mater Chem B* 2:1009–1023
- [43] Du C, Shi J, Shi J, Zhang L, Cao S (2013) PUA/PSS multilayer coated CaCO₃ microparticles as smart drug delivery vehicles. *Mater Sci Eng C* 33:3745–3752
- [44] Shi J, Wang X, Xu S, Wu Q, Cao S (2016) Reversible thermal-tunable drug delivery across nano-membranes of hollow PUA/PSS multilayer microcapsules. *J Membr Sci* 499:307–316
- [45] Song Z, Liu Y, Shi J, Ma T, Zhang Z, Ma H, Cao S (2018) Hydroxyapatite/mesoporous silica coated gold nanorods with improved degradability as a multi-responsive drug delivery platform. *Mater Sci Eng C* 83:90–98
- [46] Guo YJ, Wang YY, Chen T, Wei YT, Chu LF, Guo YP (2013) Hollow carbonated hydroxyapatite microspheres with mesoporous structure: hydrothermal fabrication and drug delivery property. *Mater Sci Eng C* 33:3166–3172
- [47] Wang P, Chen S, Cao Z, Wang G (2017) NIR light-, temperature-, pH-, and redox-responsive polymer-modified reduced graphene oxide/mesoporous silica sandwich-like nanocomposites for controlled release. *ACS Appl Mater Interfaces* 9:29055–29062
- [48] Ma X, Shi X, Bai S, Gao YE, Hou M, Han MY, Xu Z (2017) Acid-activatable doxorubicin prodrug micelles with folate-targeted and ultra-high drug loading features for efficient antitumor drug delivery. *J Mater Sci* 53:892–907. <https://doi.org/10.1007/s10853-017-1546-z>